Structure and cell viability analysis of *Actinobacillus succinogenes* biofilms as biocatalysts for succinic acid production

Sekgetho Charles Mokwatlo[a], Willie Nicol[a]

[a]Department of Chemical Engineering, University of Pretoria, Lynnwood Road,

Hatfield, 0002, Pretoria, South Africa

Postal address: Department of Chemical Engineering, University of Pretoria,

Private Bag X20, Hatfield, 0028, South Africa

E-mail addresses:

Prof. W. Nicol: willie.nicol@up.ac.za : corresponding author

Mr. S.C Mokwatlo: u11119072@tuks.co.za

Abstract

Biofilms of *Actinobacillus succinogenes* have demonstrated exceptional capabilities as biocatalysts for high productivity, titre, and yield production of succinic acid. This work gauges the effectiveness of these biofilms through analysis of the structure and cell viability of biofilms by using confocal scanning laser microscopy, scanning electron microscopy and image analysis software. The structure of the mature six-day-old biofilms of *A. succinogenes* was characterized by amorphous cell microcolonies of variable area and shape, with a mean thickness of 92±35 μm and low surface area to volume ratios of 0.25±0.07 μm^2 μm^{-3}. Biofilm surface area coverage was low near the base (33±13%) but increased towards the outer layer. Despite the presence of water channels at the deeper portions of the biofilm, a greater portion of inactive cells was closest to the attachment surface and 65±2% of the biofilm consisted of dead cells. In this way, a cell viability gradient existed where the outer layer exhibits a greater fraction of active cells compared to the base layer. Biofilm cells underwent a phenotypic change, expressing a filamentous cell morphology different from rod-like morphology of suspended cells. The filamentous morphology permits extensive cell entanglements within a microcolony which may add to the intactness of microcolonies.

Keywords

Actinobacillus succinogenes; succinic acid; biofilm architecture; cell viability; CSLM; SEM

1. Introduction

Biofilms epitomize the most successful mode of bacterial life. In this mode, juxtaposed cell colonies covered in a gel-like matrix, collectively express enhanced tolerance to harsh conditions, resistance to antimicrobial activity, and long-term activity among other known favorable traits [1]. As such, the use of biofilms as bioprocess production platforms is an interesting area with much potential. One such potential bioprocess is the production of succinic acid (SA) platform chemical using bioreactors of *Actinobacillus succinogenes* biofilms. The production of SA with *A. succinogenes* has been subjected to intense research scrutiny in the open literature, exploring steady-state metabolic flux distributions at various fermenter conditions [2–5], rate comparisons of biofilm and suspended modes [3,5], fermentations of various sugar types including hydrolysate streams [6–8], and using different reactor configurations [3,9,10]. Maharaj et al. [5] observed that specific succinic acid (SA) productivity (per mass of biomass) decreased with increasing concentrations of SA, which was attributed to possible changes in the composition of the biofilm or fraction of the metabolically active cells within the biofilm. However, to date, the structure and physiological state of *A. succinogenes* biofilms have not been studied in literature. To further develop the understanding of this biofilm process, an attempt should be made to incorporate a description of the physical properties of the biofilm. This will complement the large body of research available on the biofilm process and will aid in further manipulation and optimization.

In this study, six-day-old biofilms of *A. succinogenes*—grown in a continuous lab scale fermenter for succinic acid production—are studied by microscopic visualisation using confocal scanning laser microscopy (CSLM) and scanning electron microscopy (SEM). The structure of the biofilms, as revealed by micrographs and quantitative image analysis, is presented. Cell morphology differences between sessile cells and suspended cells are discussed along with the activity of cells within the biofilm. Shear rates, medium composition, steady state SA titre prior to sampling, as well as fermenter operation period and procedure, were all kept constant.

2. Materials and Methods

2.1. Microorganism and fermentation medium

Wild-type *Actinobacillus succinogenes* 130Z (DSM No. 22257; ATCC No. 55618) was acquired from the German Collections of Microorganisms and Cell Cultures (Braunschweig, Germany). Inoculum was prepared as previously described by [9]. All chemicals were obtained from Merck KGaA (Darmstadt, Germany) unless otherwise stated. The medium was made up of three parts: the nutrient and salts solution, a phosphate buffer, and the glucose solution. The glucose concentration was kept at 40 g L^{-1}. The phosphate buffer consisted of 3.2 g L^{-1} KH_2PO_4 and 1.6 g L^{-1} K_2HPO_4. The nutrient and salt solution was composed of (in g L^{-1}) 10.0 of clarified corn steep liquor (Sigma-Aldrich, St. Louis, USA), 6.0 of yeast extract, 1.0 NaCl, 0.2 $MgCl{\cdot}6H_2O$, 0.2 $CaCl2{\cdot}2H_2O$, and 10 mL L^{-1} of antifoam SE-15 (Sigma-Aldrich, Germany). CO_2 (Afrox, South Africa) was fed to the fermenter at 0.1 vvm.

2.2. Experimental setup and biofilm cultivation

Biofilm was grown using a continuous fermenter setup illustrated in Fig. S1, which is a modification of the design used by [2]. The setup allows for broth circulation from the main fermenter body, at a constant recirculation rate of 20.3 mL min^{-1} (1.8 mm s^{-1}), through a separate and removable sample compartment (Fig S1) where biofilm attaches to sample coverslips. Eight 13 mm diameter Thermanox coverslips (Thermo Fisher Scientific, Massachusetts, USA) and three 25 × 25 mm glass coverslips (Brand, Wertheim, Germany) were attached on both sides of a 5 mm slit within the sample compartment. Four wooden sticks covered with cheese cloth were inserted in the main fermenter body to provide the attachment surface for sufficient and stable biofilm growth.

Temperature and pH were controlled at 37.0 ± 0.1 °C and 6.80 ± 0.01 respectively. pH was controlled by dosing 10M NaOH in an on-off fashion using an internal relay in a Liquiline CM442 (Endress+Hauser, Gerlingen, Germany) coupled to a Ceragel CPS71D glass electrode

(Endress+Hauser, Gerlingen, Germany). The entire fermenter setup (fermenter, sample compartment, tubing and reservoirs) excluding the 10 M NaOH solution, was autoclaved at 121 °C for 60 min.

After inoculation, the fermenter was operated in batch mode for 24 h to increase cell density, thereafter it was switched to continuous mode at a low dilution rate of 0.1 h^{-1} to avoid cell washout (Bradfield and Nicol, 2016). The low dilution rate was maintained for 24 h during which biofilm accumulation became visible on the fermenter glass. After this period biofilm formation was accelerated by operating at a higher dilution rate of 0.3 h^{-1} for a 48 h period. Thereafter the dilution rate was dropped to 0.1 h^{-1} to achieve steady state operation at 15–21 g L^{-1} succinic acid. Steady state was maintained for 24 h before sampling. It thus took six days to cultivate mature biofilms and to sample at desired acid conditions. Broth concentrations at steady state are shown in Table 1. A total of three steady state conditions were achieved in three separate experimental runs. In this way, there was a total of three biofilm sampling events.

2.3. Image Acquisition

For confocal scanning laser microscopy, coupons were stained using Baclight LIVE/DEAD bacterial viability (Thermo Fisher Scientific, USA) stains as per instruction and mounted. The staining method considers cells with intact membranes to be viable and those with disrupted membranes to be dead. Biofilm images were acquired using an LSM 510 Meta laser scanning confocal microscope (Zeiss, Germany) and were further processed with a ZEN 2.3 Lite Image Processor (Zeiss, Germany) software. Biofilm samples were observed with the 10× (Plan-Neofluar 10×/0.3), 40× (Plan-Neofluar 40×/1.3 Oil DIC), and 100× (Plan-Apochromat 100×/1.4 Oil DIC) objectives. Image stacks were acquired by taking a series of horizontal *xy* optical scans from the substratum surface to the top of the biofilm. A minimum of three regions on each sample coupon were scanned. An excitation wavelength of 488 nm was used and the emission fluorescence was collected at 635 nm and 500 nm. For scanning electron microscopy, briefly, sampled biofilm coupons were fixed in 2.5% glutaraldehyde/formaldehyde mixture, postfixed in 1% OsO_4, dehydrated in graded ethanol solutions, and chemically dried using hexamethydisilazane and

carbon coated according to standard procedures. Specimens were visualised with a Zeiss Crossbeam 540 SEM (Zeiss, Germany, Oberkochen).

2.4 Analytical methods

Concentrations of glucose, ethanol and organic acids in the fermenter broth were determined by High-Performance Liquid Chromatography (HPLC) as described by [9]. An Agilent 1260 Infinity HPLC (Agilent Technologies, USA), equipped with an RI detector and a 300 mm × 7.8 mm Aminex HPX-87H ion exchange column (Bio-Rad Laboratories, USA) was used.

2.5 Digital image analysis

CSLM image stacks were processed using the COMSTAT [11] digital image analysis software to generate quantitative data relating to the biofilm structure. The mean biofilm thickness, fraction area occupied by biofilm in each layer of the image stack, area distribution of microcolonies at the substratum, roughness coefficient, and surface to volume ratio were analysed. Heydorn et al. [11] gives an in-depth description these parameters and how they are computed.

The descriptive quantitative parameters of the biofilm are computed based on a biofilm sample area that is representative of the biofilm. In this study, the minimum representative biofilm sampling area for *A. succinogenes* was determined by using a method described by [12]. The result indicated that the minimum representative biofilm sampling area for *A. succinogenes* is 2×10^6 μm^2 (Fig. S2). Sufficient image acquisition area (4×10^6 μm^2) was obtained only from the samples of the third experiment. Accordingly, only images of the third experiment were used for quantitative analysis. The underlying assumption was made that the quantitative analysis of the third sample was representative of the three samples given the consistent biofilm cultivation procedure and the similar steady state SA titres (Table 1).

Results and Discussion

3.1 Biofilm Architecture

Biofilms of *A. succinogenes* tend to aggregate, forming cell microcolony structures of variable area, shape, and thickness (Fig. 1), a mark of significant structural heterogeneity. CSLM and SEM images both revealed microcolony structures surrounded by an extensive network of water channels which varied in width (Fig. 1 & Fig. 2a). Typically, microcolony structures were closely spaced (Fig. 1a), however, regions of well-separated microcolony structures characterized by well-defined borders were also observed (images not shown). Cell microcolonies had smaller areas near the substratum surface and the area increased towards the top part of the biofilm, often resulting in the coalescing of proximate microcolonies to form even larger microcolonies (Fig. 2a). This observation is in good agreement with the computations of the biofilm area coverage across biofilm depth, presented in Fig. 2b, which show that low biofilm area coverage occurred near the substratum surface and increased with increasing biofilm distance from the substratum surface. Therefore, the widest water channels were found at the base of the biofilm. The observed biofilm architecture indicates that the nutrient-rich fermentation broth had some access to both the base of the biofilm and to sessile cells deeper within microcolonies through the void spaces observed between microcolonies.

Table 2 presents results for the quantitative analysis of the biofilm structure for five image stacks acquired with a 10× objective lens, totaling an area of 4.2×10^6 μm^2. Biofilm area coverage at the substratum surface was consistently low at an average of 33%. This confirmed the affinity of *A. succinogenes* biofilms to aggregate and form microcolonies at the conditions investigated, considering that flat biofilms are conventionally characterised by complete substratum surface coverage. The high average diameter and thickness (Table 2) of cell microcolonies resulted in the low surface area to volume ratios of the biofilm, given that flat biofilms have the lowest surface area to volume ratios whereas filamentous biofilms have the highest [11]. The roughness co-efficient (R_a^*) is commonly used as a measure of the variation in biofilm thickness. Flat biofilms will have low Ra* magnitudes whereas filamentous biofilms will have high R_a^* magnitudes. For

example, Heydorn et al. [11] and Murga [13] reported R_a^* values in the range of 0.15 to 0.35 for flat and uniform biofilm structure of *Pseudomonas aeruginosa*, whereas filamentous and elongated-microcolony structure of *Pseudomonas putida* biofilms had R_a^* values in the range of 0.73 to 1.82. In this way, an increased number of microcolonies per area increases the R_a^* parameter. The observed architecture of *A. succinogenes* biofilms is neither filamentous nor flat, but a closely spaced distribution of large microcolonies interspersed with void spaces, hence a R_a^* range of 0.31– 0.91 which lies between the two extremes of flat and filamentous biofilms. The results of the quantitative analysis are thus consistent with the visually observed biofilm architecture.

3.2 Biofilm cell morphology

Suspended cells and detached biofilm fragments in the fermenter effluent were visualized with a light microscope. The morphology of sessile cells is remarkably different from that expressed by planktonic cells (Fig. 3). Planktonic cells were rod-shaped (1–2 μm × 4–5 μm) whereas sessile cells expressed an elongated rod morphology (0.5–1 μm × 10–100 μm) as clearly observed in Fig. 3a and b. The sessile cell morphology result in higher surface area to volume ratios than the planktonic cells (when considering equal cell volumes). This has potential to enhance the nutrient uptake capability of the sessile cells. Furthermore, the filamentous morphology of sessile cells allows for extensive entanglement of cells within a microcolony and could contribute to the structural stability of the microcolonies. In contrast, the short rod shape of the planktonic cells will not allow for any form of entanglement. The observed elongation of sessile cells, called filamentation, has been noted for several bacteria [14–16]. It has been suggested that filamentation is a bacterial adaptive mechanism for survival, which is triggered by environmental and genetic stresses [15]. It is possible that the high salinity environments of the fermenter, caused by pH control with NaOH, triggered the filamentation of cells as elongated cells have been observed under high salinity conditions [16].

In Fig. 4, SEM biofilm images obtained at high magnification revealed extensive cell–cell and cell–surface cylindrical connection “wires” of constant diameter (20–30 nm). A closer inspection

revealed that these connection wires extended from the cell surface, as indicated in Fig. 4b. Numerous wires extended from the surface of each sessile cell and connected either to other cells or to the substratum surface, depending on the location of the cell in the microcolony. For sessile cells near the substratum surface, most connection wires contacted the substratum surface, as shown in Fig. 4a. Furthermore, considerable material deposits were observed on the surface of sessile cells which gave them a rugged-looking appearance in Fig. 4. The presence of the wire-like structures is characteristically noted in many biofilm investigations using traditional SEM sample preparation techniques [17–20]. Dohnalkova et al. [18] speculated that these wire-like structures are collapsed EPS material, formed because of viscoelastic deformation of the EPS during the dehydration steps of traditional SEM sample preparation. Nonetheless, Alhede et al. [17], who compared conventional SEM with cryo-SEM and Environmental-SEM (ESEM), speculated that they could be either the condensed EPS material, or actual polymer substances found underneath the EPS matrix. This was mainly because when using cryo-SEM and ESEM, the hydrated EPS matrix is preserved, which prevents observation of internal EPS matrix components, and thus the absence or presence of wire structures could not be confirmed.

3.3 Biofilm cell viability

A close inspection of the biofilm with a 100× objective lens showed that the biofilm became increasingly composed of living cells towards top part of the biofilm as seen in Fig. 5. Moreover, in the bottom 20 μm layer of the biofilm, approximately 80% of the biofilm was dead as revealed by a red and green pixel count with a custom Matlab® program. Orthographic views (*xy*, *xz* and *yz*) of image stacks acquired with a 10× objective lens showed that there was a random scatter of live and dead cells in the *xy* planes, with most of the cells being dead (Fig. S3). However, in the *xz* and *yz* planes, a distinct dead (red) layer of biofilm near the substratum surface and an active (green) layer close to the top of the biofilm were observed (Fig. S3). The mean of the average percentage dead cell counts —for five image stacks acquired with a 10× objective lens— revealed that 65±2% of the entire biofilm was composed of dead cells. In this way, regardless of the presence of water channels at the base of the biofilm, two thirds of the biofilm consisted of dead cells with most the dead cells located near the base of the biofilm.

The biofilm was subjected to high acid conditions (see Table 1) prior to sampling. Since mass transfer in the biofilm is reported to be dominantly diffusion controlled [21], it can be expected that catabolite concentrations will increase with biofilm depth while substrate concentrations will decrease. The deeper layers of the biofilm are thus exposed to the harshest and growth-limiting environmental conditions. In addition, the deeper biofilm cells are the oldest given that colonisation starts from the substratum interface. Accordingly, cell death most likely occurs in the deeper layers due to prolonged exposure to high acid titres as reflected in the results of Fig. 5. The results suggest that operation at high SA titres comes at a cost of reduced overall biofilm activity. Reported mass based SA productivity in biofilm fermenters thus become severely underestimated at high SA titres, hence the observed trends of decreasing mass based SA productivity with increasing SA titres [3,5]. Coupling mass based productivity calculations with viability analysis may give a more accurate trend.

4. Conclusions

Succinate-producing biofilms of *A. succinogenes*, grown in a fermenter, were analyzed, and visualized. Cells within a biofilm tended to aggregate, forming microcolonies with lower bases of biomass near the substratum surfaces but which enlarged towards the biofilm-liquid interface. Microcolonies were surrounded with an extensive network of channels, with the widest channels found at the substratum surface, as evidenced by low area coverage by the biofilm at the substratum surface. A high percentage of dead cells was near the substratum regardless of the presence of water channels at the base of the biofilm. However, the biofilm was increasingly composed of living cells towards the biofilm-liquid interface. Cells within biofilms expressed a distinct morphology compared to suspended cells as the biofilm cells were much longer and thinner.

Acknowledgements

The financial assistance of the National Research Foundation (NRF) of South Africa towards this research is hereby acknowledged. The financial assistance of the Sugar Milling Research Institute via the Step-Bio program is hereby gratefully acknowledged.

References

[1] R. Gross, B. Hauer, K. Otto, A. Schmid, Microbial biofilms: new catalysts for maximizing productivity of long-term biotransformations., Biotechnol. Bioeng. 98 (2007) 1123–34. doi:10.1002/bit.21547.

[2] M.F.A. Bradfield, W. Nicol, Continuous succinic acid production by Actinobacillus succinogenes in a biofilm reactor: Steady-state metabolic flux variation, Biochem. Eng. J. 85 (2014) 1–7. doi:10.1016/j.bej.2014.01.009.

[3] H.G. Brink, W. Nicol, Succinic acid production with Actinobacillus succinogenes : rate and yield analysis of chemostat and biofilm cultures, (2014) 1–12. doi:10.1186/s12934-014-0111-6.

[4] J. Herselman, M.F.A. Bradfield, U. Vijayan, W. Nicol, The effect of carbon dioxide availability on succinic acid production with biofilms of Actinobacillus succinogenes, Biochem. Eng. J. 117 (2017) 218–225. doi:10.1016/j.bej.2016.10.018.

[5] K. Maharaj, M.F.A. Bradfield, W. Nicol, Succinic acid-producing biofilms of Actinobacillus succinogenes: Reproducibility, stability and productivity, Appl. Microbiol. Biotechnol. 98 (2014) 7379–7386. doi:10.1007/s00253-014-5779-3.

[6] M.F.A. Bradfield, A. Mohagheghi, D. Salvachúa, H. Smith, B.A. Black, N. Dowe, G.T. Beckham, W. Nicol, Continuous succinic acid production by Actinobacillus succinogenes on xylose - enriched hydrolysate, Biotechnol. Biofuels. (2015) 1–17. doi:10.1186/s13068-015-0363-3.

[7] M.F.A. Bradfield, W. Nicol, Continuous succinic acid production from xylose by Actinobacillus succinogenes, Bioprocess Biosyst. Eng. 39 (2016) 233–244. doi:10.1007/s00449-015-1507-3.

[8] D. Salvachúa, A. Mohagheghi, H. Smith, M.F.A. Bradfield, W. Nicol, B.A. Black, M.J. Biddy, N. Dowe, G.T. Beckham, Succinic acid production on xylose-enriched biorefinery streams by Actinobacillus succinogenes in batch fermentation., Biotechnol. Biofuels. 9 (2016) 28. doi:10.1186/s13068-016-0425-1.

[9] M. Il Kim, Continuous Production of Succinic Acid Using an External Membrane Cell Recycle System, J. Microbiol. Biotechnol. 19 (2009) 1369–1373. doi:10.4014/jmb.0903.03034.

[10] S.E. Urbance, A.L. Pometto, A. a Dispirito, Y. Denli, Evaluation of succinic acid continuous and repeat-batch biofilm fermentation by *Actinobacillus succinogenes* using plastic composite support bioreactors., Appl. Microbiol. Biotechnol. 65 (2004) 664–70. doi:10.1007/s00253-004-1634-2.

[11] A. Heydorn, A.T. Nielsen, M. Hentzer, M. Givskov, B.K. Ersbøll, S. Molin, Quantification of biofilm structures by the novel computer program COMSTAT, (2016) 2395–2407.

[12] V.P. Venugopalan, M. Kuehn, M. Hausner, D. Springael, A. Wilderer, S. Wuertz, P.A. Wilderer, Architecture of a Nascent Sphingomonas sp . Biofilm under Varied Hydrodynamic Conditions Architecture of a Nascent Sphingomonas sp . Biofilm under Varied Hydrodynamic Conditions †, 71 (2005) 2677–2686. doi:10.1128/AEM.71.5.2677.

[13] R. Murga, P.S. Stewart, D. Daly, Quantitative analysis of biofilm thickness variability, Biotechnol. Bioeng. 45 (1995) 503–510. doi:10.1002/bit.260450607.

[14] R. Janissen, D.M. Murillo, B. Niza, P.K. Sahoo, M.M. Nobrega, C.L. Cesar, M.L.A. Temperini, H.F. Carvalho, A.A. de Souza, M.A. Cotta, Spatiotemporal distribution of different extracellular polymeric substances and filamentation mediate Xylella fastidiosa adhesion and biofilm formation., Sci. Rep. 5 (2015) 9856. doi:10.1038/srep09856.

[15] S.S. Justice, D. a Hunstad, L. Cegelski, S.J. Hultgren, Morphological plasticity as a bacterial survival strategy., Nat. Rev. Microbiol. 6 (2008) 162–168. doi:10.1038/nrmicro1820.

[16] K.K. Sakimoto, C. Liu, J. Lim, P. Yang, Salt-Induced Self-Assembly of Bacteria on Nanowire Arrays, (2014). doi:10.1021/nl502946j.

[17] M. Alhede, K. Qvortrup, R. Liebrechts, N. Høiby, M. Givskov, T. Bjarnsholt, Combination of microscopic techniques reveals a comprehensive visual impression of biofilm structure and composition, Immunol. & Med. Microbiol., (2012). doi:10.1111/j.1574-695X.2012.00956.x.

[18] A.C. Dohnalkova, M.J. Marshall, B.W. Arey, K.H. Williams, E.C. Buck, J.K. Fredrickson, Imaging Hydrated Microbial Extracellular Polymers : Comparative Analysis by Electron Microscopy □ †, 77 (2011) 1254–1262. doi:10.1128/AEM.02001-10.

[19] R.C. Hunter, T.J. Beveridge, High-Resolution Visualization of Pseudomonas aeruginosa PAO1 Biofilms by Freeze-Substitution Transmission Electron Microscopy, 187 (2005) 7619–7630. doi:10.1128/JB.187.22.7619.

[20] B. Little, P. Wagner, R. Ray, R. Pope, S. Raymond, Biofilms : an ESEM evaluation of artifacts introduced during SEM preparation, 8 (1991) 213–221.

[21] M.C.M. Van Loosdrecht, J.J. Heijnen, H. Eberl, J. Kreft, C. Picioreanu, Mathematical modelling of biofilm structures, Antonie Leeuwenhoek, (2002) 245–256.

Captions

Figure 1: (a) CSLM 3D reconstruction of optical scans of a z stack showing clustered cell microcolonies as observed from the top and at an angle. (b) SEM topographical view also showing cell microcolonies surrounded by water channels. Scale bar in (b) denotes 100 µm.

Figure 2: Areal coverage by biofilm as function of biofilm depth. (a) CSLM optical scans of the biofilm in the xy plane starting from the substratum surface at z = 0 µm. (b) Cross sectional coverage of biofilm as function of biofilm depth. Scale bar in (a) denotes 20 µm.

Figure 3: Sessile cells expressed a distinct cell morphology compared to planktonic cells. (a) Planktonic cells were rod-shaped with a width range of 1 – 2 µm and length range of 4 – 5 µm. (b) Sessile cells expressed an elongated rod morphology, with lengths ranging from 5 –100 µm and a thickness range of 0.5 – 1 µm. The elongated sessile cells were also observed with CSLM and SEM visualisation as seen in (c) and (d) respectively. Scale bars in (a) and (b) denote 20 µm, and those in (c) and (d) denote 2 µm.

Figure 4: SEM visualisation revealed the presence of thin constant diameter, wire-like structures, approximately 20 – 30 nm in diameter, interconnecting cell surfaces to substratum surfaces (a), and to other cell surfaces (b). Scale bar in (a) denotes a 100 nm, and that in (b) denotes 200 nm

Figure 5: CSLM optical scans across a biofilm depth showing an increasing gradient of living (green) cells starting from the substratum surface at z = 0 µm to the biofilm-liquid interface of the microcolony at z = 50 µm.

Figure 1

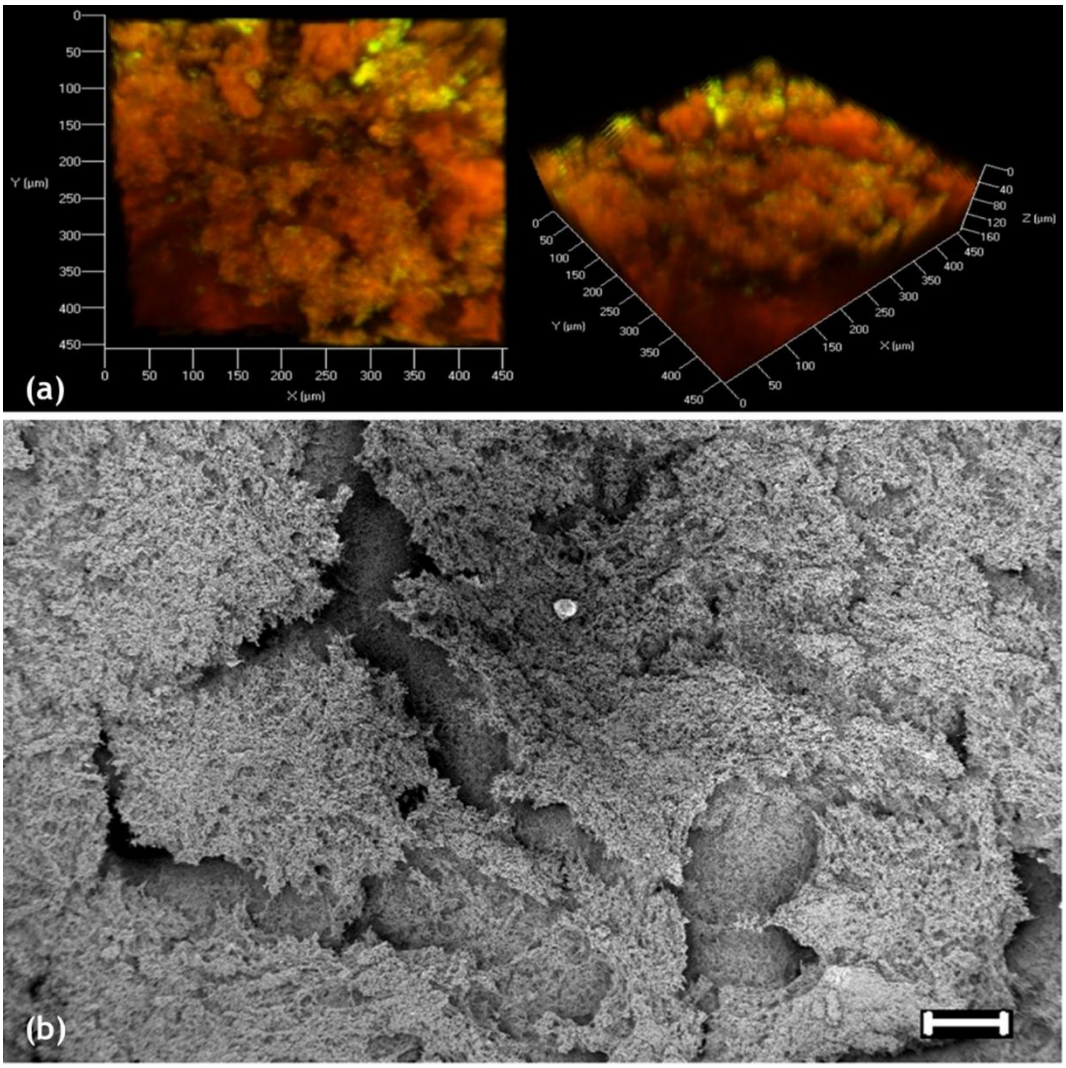

Figure 2

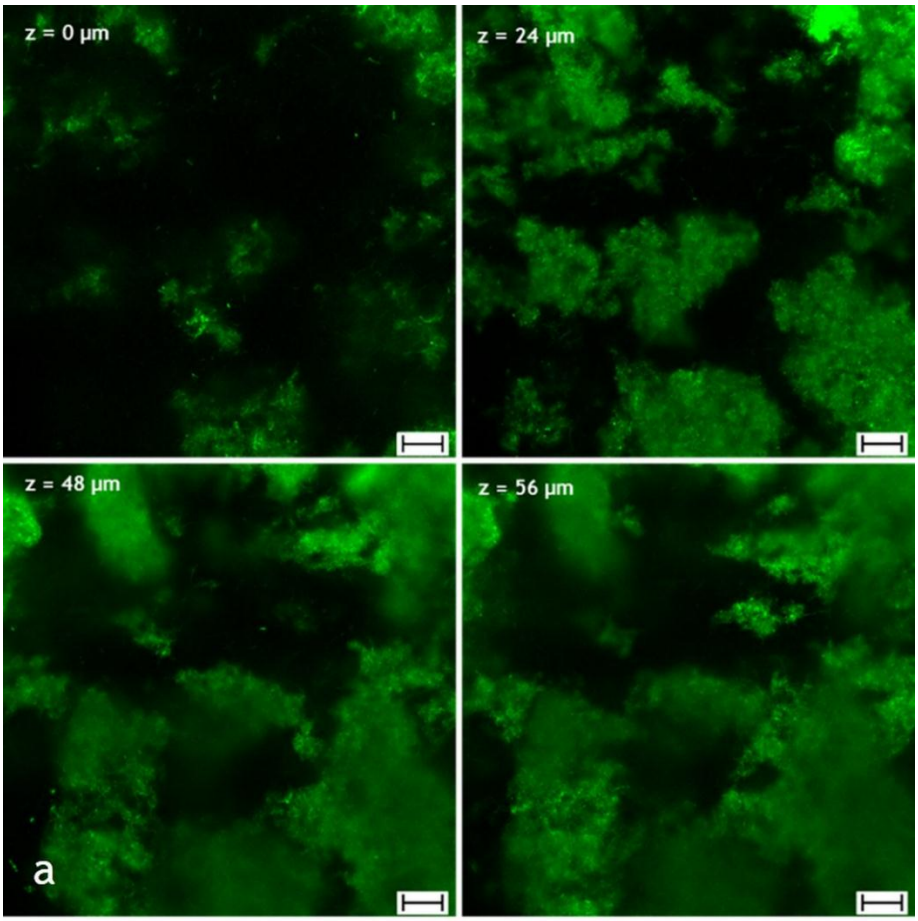
z = 0 µm
z = 24 µm
z = 48 µm
z = 56 µm
a

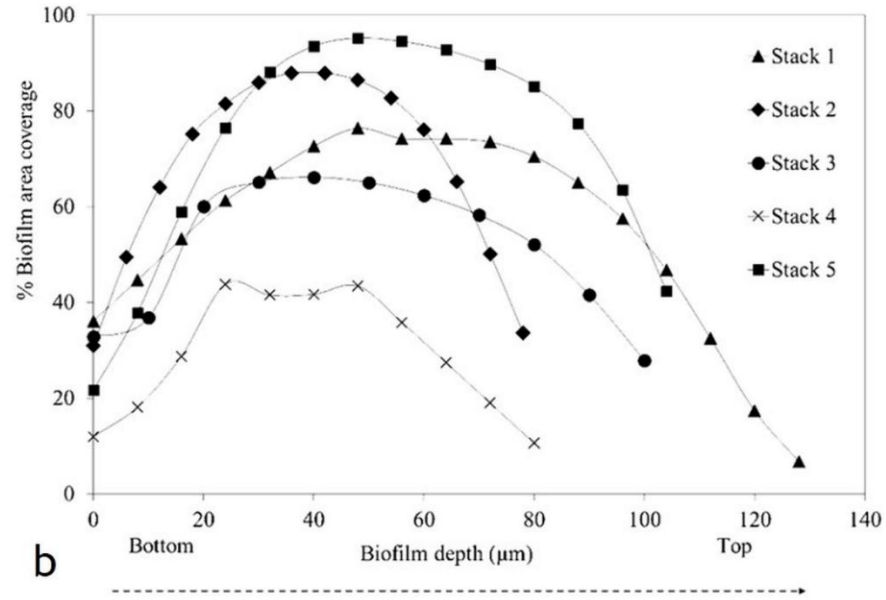
% Biofilm area coverage
Biofilm depth (µm)
Bottom
Top
Stack 1
Stack 2
Stack 3
Stack 4
Stack 5
b

Figure 3

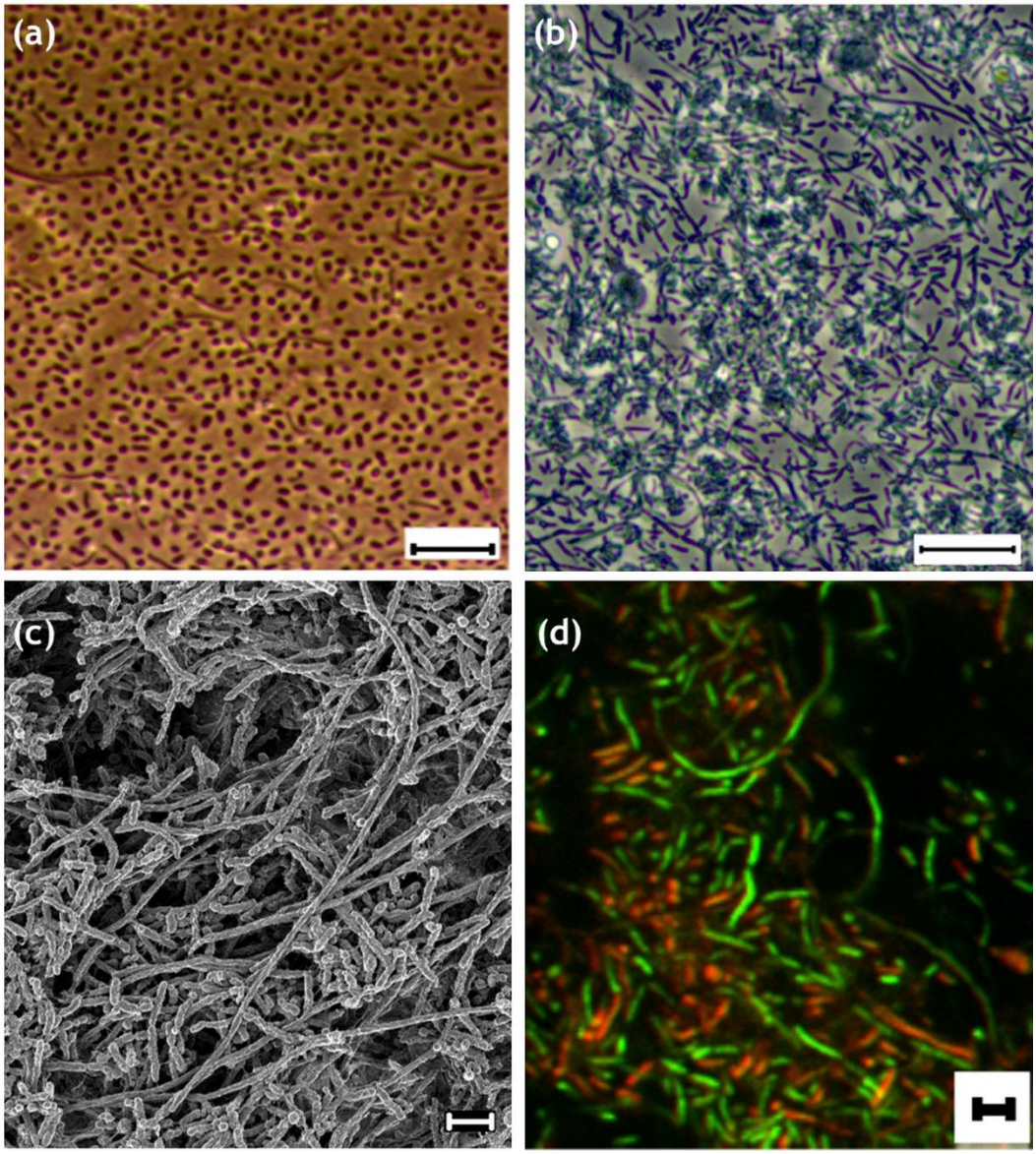

Figure 4

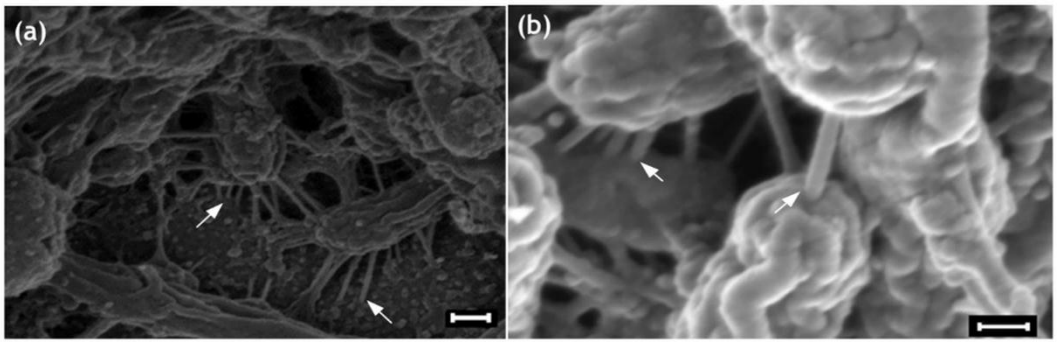

Figure 5

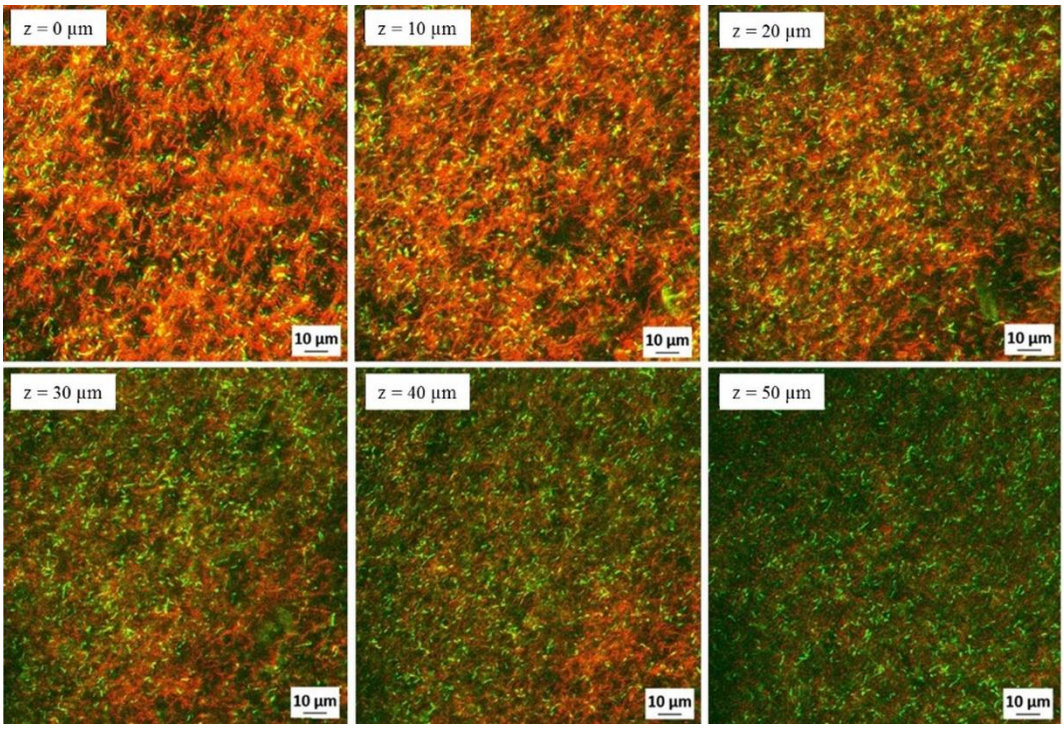

Supplementary Figures

Figure S1

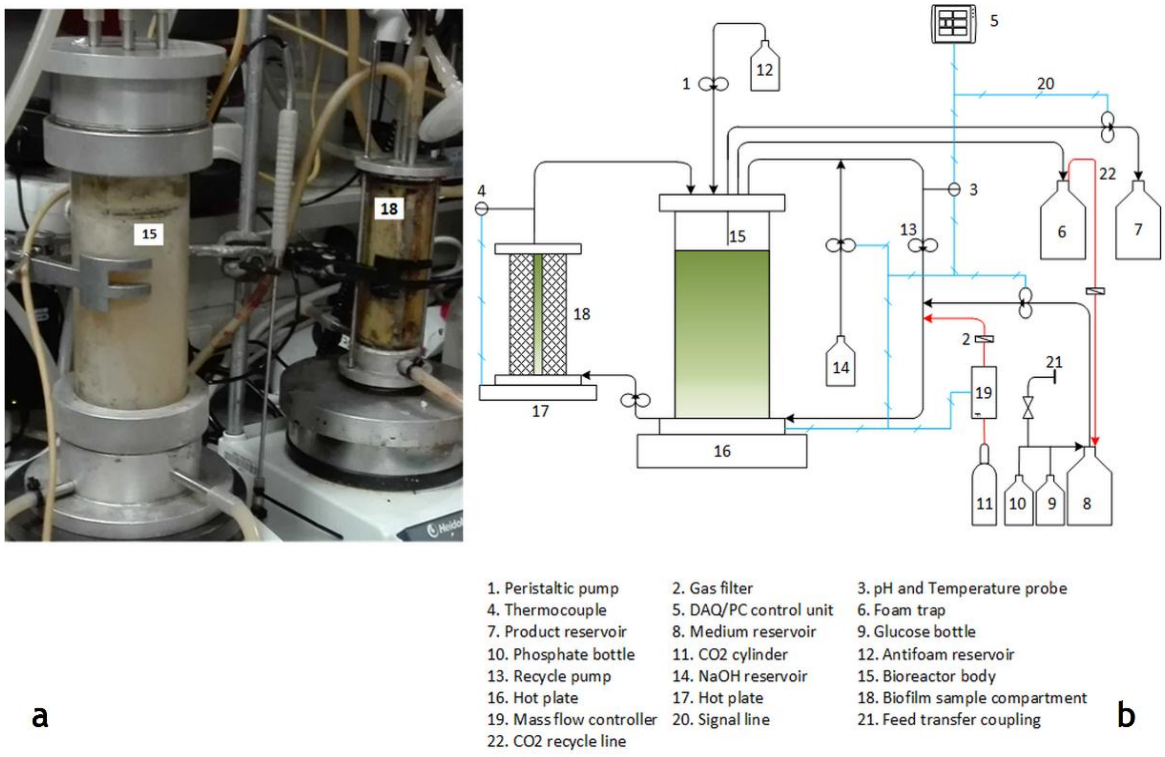

Figure S1: (a) The bioreactor and sample compartment, biofilm can be seen on the glass walls. (b) The schematic of the diagram of the fermentation setup. Not to scale. Not all gas vents are shown.

Figure S2

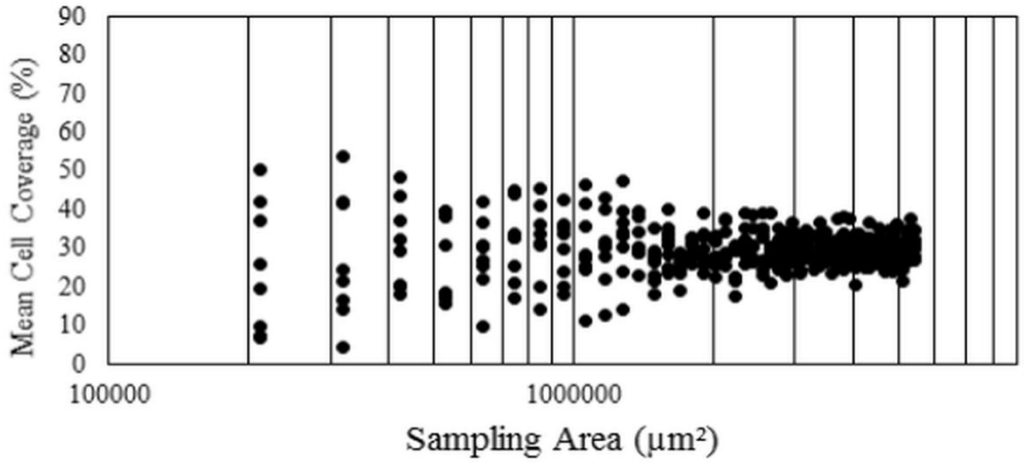

Figure S2: Determination of minimum representative biofilm sampling area for *A. succinogenes* using substratum coverage by biofilm as a determinative parameter. The percentage substrate surface covered becomes independent of sampled area after a sampled biofilm area of approximately 2×10^{6} μm^{2}.

Figure S3

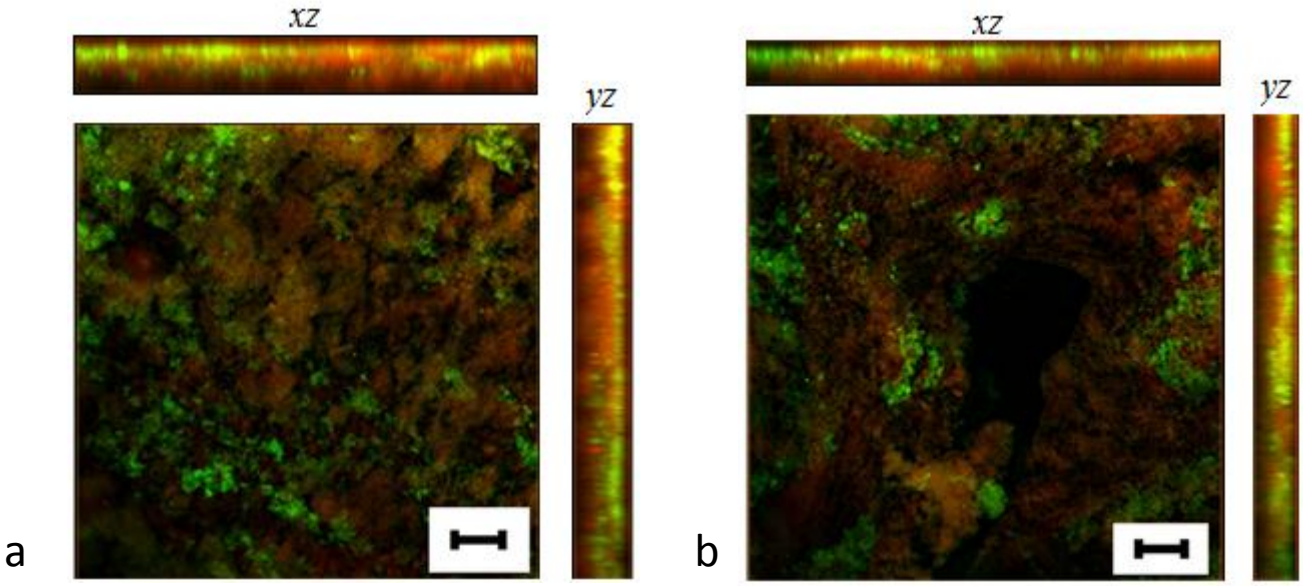

Figure S3: CSLM orthographic views of the *xy*, *xz* and *yz* planes showing the variation of dead and living cells in the horizontal plane and vertical plane. Observe a red (dead) layer of biofilm near the bottom of vertical plane views. Scale bar indicate a 100 µm.